

# The Role of Short-Range Disorder in BaWO<sub>4</sub> Crystals in the Intense Green Photoluminescence

Marcos Anicete-Santos,<sup>\*,†</sup> Francini C. Picon,<sup>‡</sup> Cláudio N. Alves,<sup>†</sup> Paulo S. Pizani,<sup>‡</sup> José A. Varela,<sup>§</sup> and Elson Longo<sup>§</sup>

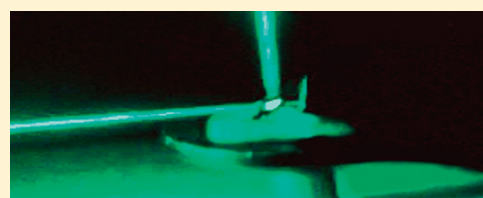
<sup>†</sup>Laboratório de Planejamento e Desenvolvimento de Fármacos - LPDF, Universidade Federal do Pará - UFPA, P.O. Box 11101, 66075-110, Belém, PA, Brazil

<sup>‡</sup>Universidade Federal de São Carlos - UFSCAR, P.O. Box 676, 13565-905, São Carlos, SP, Brazil

<sup>§</sup>LIEC, Instituto de Química, UNESP, P.O. Box 355, 14801-907, Araraquara, SP, Brazil

**S** Supporting Information

**ABSTRACT:** An intense and broad visible photoluminescence (PL) band was observed at room temperature in short-range disordered BaWO<sub>4</sub> crystals. The scheelite crystalline BaWO<sub>4</sub> powders prepared by the polymeric precursor method and annealed at different temperatures were structurally characterized by means of X-ray diffraction and Fourier transform (FT) Raman spectroscopy measurements. Quantum-mechanical calculations indicated that the disorder at short range only of Ba atoms in the BaWO<sub>4</sub> lattice has a very important role in the charge transfer involved in the intense green PL emission. This indication was detected and confirmed by means of FT Raman spectroscopy measurements. The experimental and theoretical results are in good agreement, both showing the specific type of structural disorder that is the most favorable condition for generating the most intense green PL emission in the scheelite BaWO<sub>4</sub> lattice.



## INTRODUCTION

The technological demand in light-emitting devices for displays and communication poses challenges to scientific research of optical properties. In particular, the barium and strontium tungstate scheelite crystals are prospective materials for application of Raman converters, lasers, and amplifiers.<sup>1–8</sup> Specifically, the barium tungstate BaWO<sub>4</sub> crystal has been considered as a unique Raman crystal for a wide variety of pump pulse durations from nanoseconds to picoseconds for the generation of the frequency shifted Raman laser pulses.<sup>9,10</sup>

PL is the most studied optical property. Numerous investigations of the PL property of scheelite tungstate crystals have been carried out for several decades.<sup>11–32</sup> Among the scheelite crystals, the PbWO<sub>4</sub> tungstate is the most investigated crystal in terms of its PL property.<sup>12–24,28,33–39</sup> The understanding of the PL property in scheelite crystals is still being discussed<sup>23,40</sup> regarding the contribution of color centers to PL emission bands, mainly to the green emission band. Blasse et al.<sup>12</sup> and Korzhik's group<sup>14,17,26,41</sup> concluded that the green emission originates from the (WO<sub>3</sub> + F) center in the undoped scheelite crystal, where F is an electron bound to a negative ion vacancy. Sokolenko et al.<sup>42</sup> attributed green-red emission to (WO<sub>3</sub>·V<sub>O</sub>) oxygen-deficient complexes, and Sinelnikov et al.<sup>43</sup> suggested that the WO<sub>4</sub> tetrahedra distorted upon the formation of oxygen vacancies V<sub>O</sub> in the scheelite structure is responsible for the green luminescence band. On the other hand, Shi et al.<sup>25,40,44</sup> suggest the (WO<sub>4</sub> + O<sub>i</sub>) center as the green luminescence center, whereas Huang et al.<sup>45</sup> conclude that

the interstitial oxygen O<sub>i</sub> in the scheelite lattice enhances the green luminescence.

Although the optical properties of BaWO<sub>4</sub> tungstate crystals have been studied intensively, the intense PL property at room temperature is rarely reported in undoped BaWO<sub>4</sub> crystals.<sup>46–49</sup>

In this article, we present measurements of the intense and broad visible PL band at room temperature in structurally disordered BaWO<sub>4</sub> powder at short range. The BaWO<sub>4</sub> powder samples were prepared using the polymeric precursor method.<sup>50,51</sup> This process offers advantages over several synthesis techniques, such as low cost, good compositional homogeneity, high purity, and low processing temperatures. The origin of the intense and broad PL band of the BaWO<sub>4</sub> compound containing short-range disorder in its lattice is also investigated in terms of electronic structure calculations realized in the framework of ab initio periodic quantum-mechanical techniques. The aim of our synergistic strategy between experimental and theoretical results is not to explain all the possible PL mechanisms that occur during the photon excitation and decay processes, given that many valid hypotheses already exist in the literature, but to discuss the contribution of structural disorder at short range to the green PL emission and why it provides favorable conditions for the generation of an intense and broad PL band.

**Received:** January 28, 2011

**Revised:** May 19, 2011

**Published:** May 19, 2011

## EXPERIMENTAL SECTION

BaWO<sub>4</sub> was obtained by the polymeric precursor method.<sup>38,50–52</sup> A flow chart representing the synthesis route of BaWO<sub>4</sub> used in this study is outlined in the Supporting Information. Tungsten citrate was prepared by the dissolution of  $5 \times 10^{-3}$  mol of tungstic acid (H<sub>2</sub>WO<sub>4</sub>, 99% purity, Aldrich) in 80 mL of an aqueous solution of citric acid (H<sub>3</sub>C<sub>6</sub>H<sub>5</sub>O<sub>7</sub>, Mallinckrodt, 99%) under constant stirring at 60–80 °C to homogenize the tungsten citrate solution. After homogenization of this solution,  $5 \times 10^{-3}$  mol of barium nitrate (Ba(NO<sub>3</sub>)<sub>2</sub>, 99.5% purity, Aldrich) was dissolved and a stoichiometric amount added to the tungsten citrate solution. The complex was well stirred for several hours at 60–80 °C to produce a clear, homogeneous solution. After the solution was homogenized, ethylene glycol was added to promote the citrate polymerization by polyesterification. With continued heating at 80–90 °C, the viscosity of the solution increased, albeit devoid of any visible phase separation. The molar ratio between barium and tungsten cations was 1:1. The citric acid/ethylene glycol mass ratio was set to 60:40. After partial evaporation of the water, the resin was heat-treated at 300 °C for 2 h, in a static atmosphere, leading to the partial decomposition of the polymeric gel, forming an expanded resin, constituted of partially pyrolyzed material. The product was removed from the beaker and deagglomerated. Deagglomeration was performed in this manner using high-energy milling. The powders were annealed at 500, 600, and 700 °C for 2 h in a static atmosphere and with a heating rate of 10 °C/min.

The BaWO<sub>4</sub> powder samples were structurally characterized by X-ray diffraction (XRD) using a Cu K $\alpha$  radiation source. The diffraction patterns were recorded on a Rigaku DMax2500PC model in a  $\theta$ – $2\theta$  configuration, using a graphite monochromator. The FT Raman spectra were measured using a Bruker RFS100 spectrophotometer, Nd:YAG Laser (1064 nm). The spectral dependence of optical absorbance for the crystalline BaWO<sub>4</sub> powders was measured in the reflectance mode from 200 to 800 nm, using a Cary 5G spectrophotometer. The PL spectra of the BaWO<sub>4</sub> samples were recorded with a U1000 Jobin-Yvon double monochromator coupled to a cooled GaAs photomultiplier and a conventional photon counting system. The 488 nm exciting wavelength of an argon ion laser was used, with the laser's maximum output power kept at 60 mW. A cylindrical lens was used to prevent the sample from overheating. The slit width used was 100  $\mu$ m. All measurements were taken at room temperature.

## COMPUTATIONAL METHODS

Calculations were carried out with the CRYSTAL03 package<sup>53</sup> within the framework of the density functional theory using the gradient-corrected correlation functional by Lee, Yang, and Parr, combined with the Becke3 exchange functional, B3LYP,<sup>54,55</sup> that was demonstrated by Hu et al.<sup>56</sup> to be suitable for calculating structural parameters and band structures for a wide variety of solid-state compounds. The atomic centers have been described by pseudopotential HAYWSC-31G and 8-51G\* basis sets for Ba and W, respectively. The oxygen atom is described by the all-electrons 6-31G\* basis set. The basis sets are taken from ref 57. The *k*-points sampling was chosen to be 36 points within the irreducible part of the Brillouin zone. The OPTIM<sup>58</sup> program was used for optimization calculations of *a* and *c* cell parameters. OPTIM is a general optimization tool that minimizes a chosen

**Table 1. Cell Parameters and Oxygen Fractional Atomic Positions**

	<i>a</i> (Å)	<i>c</i> (Å)	<i>x</i>	<i>y</i>	<i>z</i>
exptl <sup>a</sup>	5.6148(5)	12.721(1)	0.25(2)	0.13(2)	0.075(2)
calcd	5.56322	12.56649	0.22640	0.12332	0.04741

<sup>a</sup>Reference 59.

function, which, in this case, is the computed total energy. The initial values of the cell parameters and oxygen fractional atomic positions (*x*, *y*, and *z*) for optimization calculations were obtained from experimental data.<sup>59</sup>

The XCrysDen<sup>60</sup> program was used as a graphical tool for plotting the band structure diagrams.

## CRYSTAL STRUCTURE AND PERIODIC MODEL

The BaWO<sub>4</sub> crystallizes in a tetragonal structure, space group *I*<sub>4</sub><sup>1</sup>/*a*, known as the scheelite phase. Tungsten atoms are surrounded by four oxygen atoms in a tetrahedral configuration, and barium atoms are surrounded by eight oxygen atoms in a pseudocubic configuration. The experimental and optimized values of the cell parameters and oxygen fractional atomic positions are presented in Table 1. The fractional atomic positions of Ba and W atoms are (0, 1/4, 5/8) and (0, 1/4, 1/8), respectively.

For computational simplification, the CRYSTAL03 code works in the primitive unit cell rather than in the conventional one. We have used a primitive cell as a periodic model for representing the highly crystalline BaWO<sub>4</sub> (BWO-c). It results in 12 atoms (2 Ba, 2 W, and 8 O atoms) per primitive cell; see Figure 1a.

Our aim is to compare the electronic structure and charge distribution of the highly crystalline model with crystalline models containing disorder at short-range representing powder samples before the complete crystallization. We suppose that, before the full crystallization of the powder, that is, before the annealing temperature reaches 700 °C, the BaWO<sub>4</sub> lattice is composed of a random mixture of WO<sub>3</sub> (or distorted WO<sub>4</sub>) and regular WO<sub>4</sub> molecular groups linked by the Ba<sup>2+</sup> cations. We also suppose that some Ba coordination spheres can be distorted in the lattice.

Besides the first BWO-c highly crystalline model, we created two other periodic models to simulate the BaWO<sub>4</sub> crystals containing structural disorder at short range in their lattices. The second model was created by displacing the Ba2 atom 0.4 Å in the direction opposite to the O2 oxygen atom per unit cell, as shown in Figure 1b. This periodic model is labeled BWO-b. Starting from the previous BWO-c crystalline model, the W2 and Ba2 atoms were displaced by 0.3 and 0.4 Å in the direction opposite to the O1 and O2 oxygens, respectively. This third model is labeled BWO-bw; see Figure 1c.

Many values were tested for atomic displacements in the BWO-b and BWO-bw models. The electronic structures of the models with different displacements are similar: although the results are quantitatively different, they do not influence the conclusions of this work, which seeks to compare various disorder possibilities.

Our proposal regarding the use of these models is to offer a simple scheme enabling an understanding of the effects of structural deformations at short range in the electronic structure and charge distribution, because the most intense PL emission is

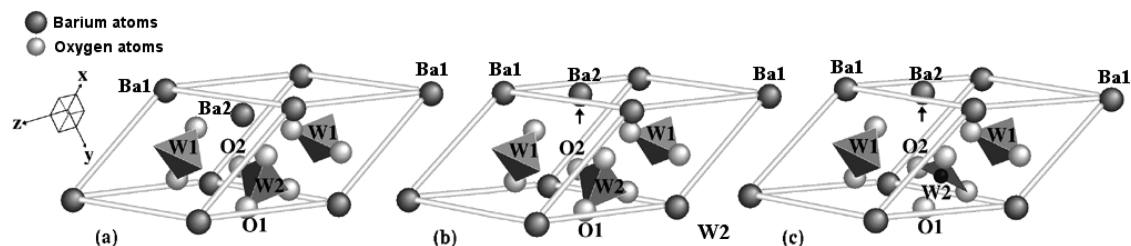


**Figure 1.** (a) BWO-c, (b) BWO-b, and (c) BWO-bw primitive unit cell periodic models of the  $\text{BaWO}_4$  structure. Arrows show the direction of  $\text{Ba}_2$  displacements.

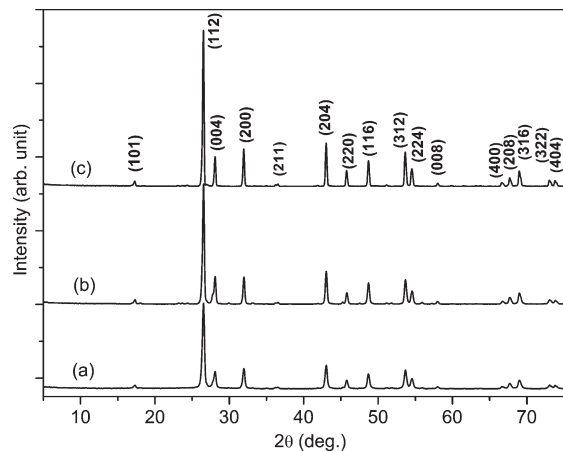


**Figure 2.** XRD patterns measured at room temperature for the  $\text{BaWO}_4$  powders heat-treated at (a) 500, (b) 600, and (c) 700 °C for 2 h in an air atmosphere.

evidenced in disordered  $\text{BaWO}_4$  lattice at short range. This strategy of models with the coexistence of different types of environments has already been successfully employed for studying PL emission in disordered structures of scheelite tungstates<sup>52,61,62</sup> and of perovskite titanates.<sup>63–67</sup> In the case of the perovskite titanates, the cationic environments had 5-fold  $\text{MO}_5$  ( $M = \text{Ti}, \text{Zr}$ ) and 6-fold  $\text{MO}_6$  coordinations.

## RESULTS AND DISCUSSION

Figure 2 presents the X-ray diffraction patterns recorded at room temperature for scheelite  $\text{BaWO}_4$  powder samples heat-treated at 500, 600, and 700 °C for 2 h in an air atmosphere. All three samples are already in the crystalline phase. No additional or intermediate phases were detected in the  $\text{BaWO}_4$  powders; all diffraction peaks are ascribed to the scheelite tetragonal structure (space group  $I4_1/a$ ,  $C_{4h}$  symmetry), which match with the ref 68 pattern.

According to Basiev et al.,<sup>5</sup> the primitive cell of the tungstate crystal at room temperature, the scheelite structure, includes two  $\text{AWO}_4$  formula units ( $A = \text{Pb}, \text{Ba}, \text{or Sr}$ ). The  $\text{WO}_4$  molecular group with  $\text{W}-\text{O}$  strong covalent bonds is the peculiarity of the scheelite structure. Because of weak coupling between the  $\text{WO}_4$  molecular group and the  $A$  cation, the vibrational modes in Raman spectra of scheelite crystals can be divided into two groups, internal and external. The internal vibrons ( $\nu_{\text{int}}$ ) correspond to the oscillations inside the  $\text{WO}_4$  molecular group with an immovable mass center:  $\nu_1(A_g)$ ,  $\nu_2(A_g)$ ,  $\nu_2(B_g)$ ,  $\nu_3(B_g)$ ,

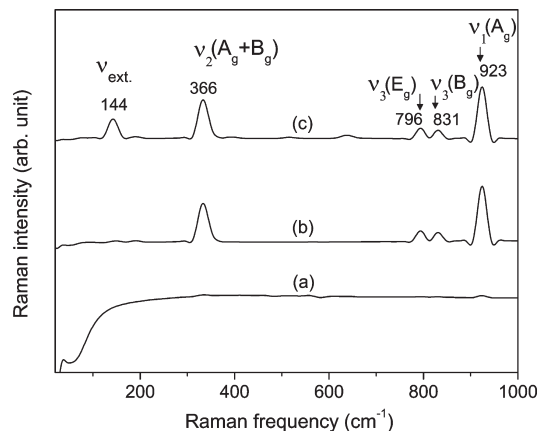


**Figure 3.** FT Raman spectra recorded at room temperature for the  $\text{BaWO}_4$  samples heat-treated at (a) 500, (b) 600, and (c) 700 °C for 2 h in an air atmosphere.

and  $\nu_3(E_g)$ . The ( $\nu_{\text{ext}}$ ) external vibrons or lattice phonon correspond to the motion of the  $A$  cation and the  $\text{WO}_4$  rigid molecular unit.<sup>5</sup>

The FT Raman spectra at room temperature of the  $\text{BaWO}_4$  powders heat-treated at 500, 600, and 700 °C are presented in Figure 3. The sample treated at 700 °C presents several peaks referring to the Raman internal modes of the  $\text{WO}_4$  tetrahedra: stretching  $\nu_1(A_g)$ ,  $\nu_3(B_g)$ , and  $\nu_3(E_g)$  and bending  $\nu_2(A_g + B_g)$ . The external mode  $\nu_{\text{ext}}$  corresponds to motion of the  $\text{Ba}$  and the  $\text{WO}_4$  rigid molecular unit,<sup>5</sup> as can be seen in Figure 3, spectrum c. The compound treated at 600 °C only presents peaks referring to the internal modes  $\nu_1(A_g)$ ,  $\nu_2(A_g + B_g)$ ,  $\nu_3(B_g)$ , and  $\nu_3(E_g)$  but does not present any external mode  $\nu_{\text{ext}}$  (see Figure 3, spectrum b), showing that the  $\text{WO}_4$  tetrahedra are ordered and the  $\text{Ba}$  are disordered at short range in the  $\text{BaWO}_4$  lattice. The sample treated at 500 °C does not present any Raman phonon mode, as presented Figure 3, spectrum a.

The X-ray diffraction data show that all three  $\text{BaWO}_4$  samples are ordered at long range. The FT Raman data show that the sample heat-treated at 500 °C is structurally disordered at short range because it does not present any Raman phonon mode. In the sample heat-treated at 600 °C, only the  $\text{Ba}$  atoms are disordered at short range in the lattice. The sample heat-treated at 700 °C shows that it is already highly ordered at short range, because it presents internal and external vibrational modes.

The absorption spectra of the  $\text{BaWO}_4$  samples annealed at 600 and 700 °C are presented in Figure 4. The gap energy values can be obtained by means of the Wood and Tauc method.<sup>69</sup> The absorption spectrum of the  $\text{BaWO}_4$  sample annealed at 500 °C was not shown in Figure 4 because this spectrum did not follow

the Wood and Tauc's law,<sup>69</sup> and for this reason, we cannot fit the law equation with the spectrum curve to calculate the gap energy. According to Wood and Tauc's law,<sup>69</sup> the absorption coefficient has the following energy dependence

$$\alpha = A(h\nu - E_{\text{gap}})^m / h\nu \quad (1)$$

where  $A$  is a constant that is different for different types of transitions, indicated by different values of  $m$  ( $m = 1/2, 2, 3/2$ , or  $3$  for allowed direct, allowed indirect, forbidden direct, and forbidden indirect electronic transitions, respectively),  $h\nu$  is the photon energy, and  $E_{\text{gap}}$  is the optical gap energy.

The gap energies of the BaWO<sub>4</sub> samples treated at 700 and 600 °C are 4.7 and 4.1 eV, respectively. Wood and Tauc associated the decrease of the gap energy value with the existence of localized states in the band gap due to structural defects.<sup>69</sup> This behavior indicates that the amount of localized states in the band gap of the sample annealed at 600 °C is greater than the amount in the band gap of the sample annealed at 700 °C, due the short-range disorder of Ba in the sample treated at 600 °C, as pointed by the Raman spectra (see spectra b and c in Figure 3).

To investigate the dominant orbitals and characters of the localized states and of bands surrounding the band gap, Figure 5 presents the calculated total and atom- and atomic orbital-

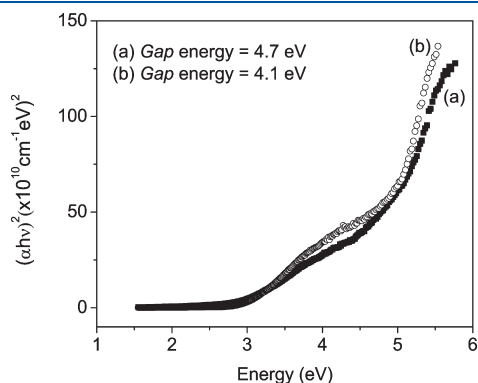


**Figure 4.** Spectral dependence on the absorbance at room temperature for the BaWO<sub>4</sub> samples heat-treated at (a) 700 and (b) 600 °C.

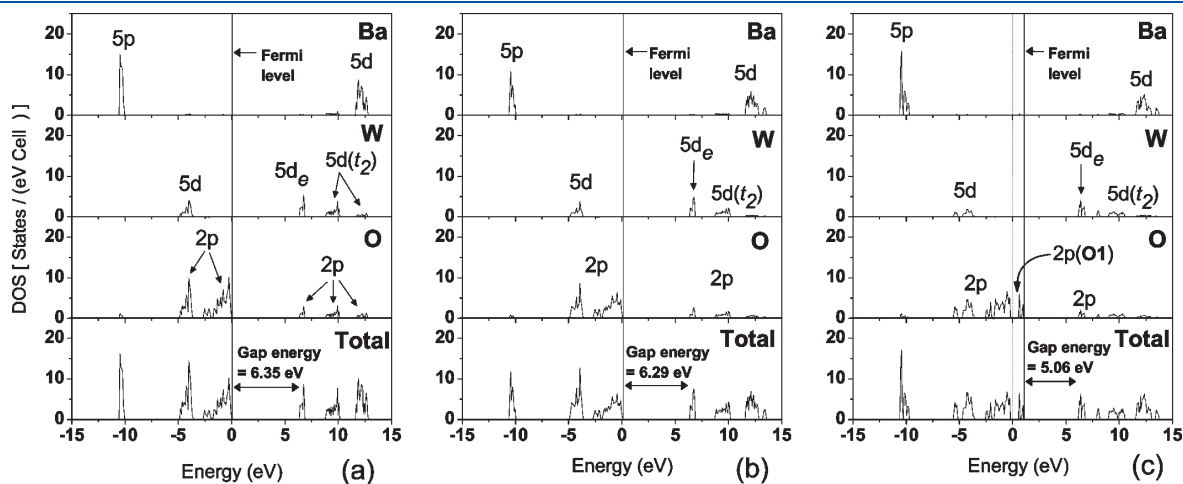
projected densities of states (DOS) for the three models with an energy ranging from  $-15$  to  $15$  eV, the zero being set at the top of the last occupied level (Fermi level) referring to the BWO-c model.

Figure 5a presents the DOS of the BWO-c model. The valence band (VB) around  $-5$  eV is mainly formed by  $2p$  (O) and  $5d$  (W) states. The upper VB is mainly formed by  $2p$  (O) states and equivalently distributed on each oxygen. The projections on the oxygens and tungstens reveal that the upper VB states are mostly nonligand  $2p$  (O) states. The conduction band (CB) is mainly formed by  $2p$  (O) and  $5d$  (W) states. The  $e$ -like (W) states ( $5d_{z^2}$ ,  $5d_{x^2-y^2}$ ) contribute in the lower portion of the CB and the  $t_2$ -like (W) states ( $5d_{xz}$ ,  $5d_{yz}$ ,  $5d_{xy}$ ) contribute around  $10$  eV. The strong covalent hybridization between the  $2p$  (O) and  $5d$  (W) states is clearly visible in the VB around  $-5$  eV and in the lower CB. The  $5p$  (Ba) states in the VB and  $5d$  (Ba) in the CB are mostly nonligand states. These results, according to Basiev's experimental work<sup>5</sup> and Porto et al.,<sup>70</sup> demonstrate that the WO<sub>4</sub> molecular group has W–O strong covalent bonds and that there are weak bonds between the WO<sub>4</sub> groups and the A (Ba) cations. The gap energy in this model is  $6.35$  eV.

Figure 5b presents the DOS of the BWO-b model, in which only the Ba were displaced in each primitive cell. The contributions of the states are very similar to the DOS in the BWO-c model, because the Ba displacement causes a slight electronic perturbation due to the weak bonds on Ba. The gap energy decreases slightly to  $6.29$  eV.

Figure 5c presents the DOS of the BWO-bw model. The electronic structure is strongly perturbed by the W2 displacement (see Figure 1c), causing the increase of structural disorder degree due to breaking of the W–O strong covalent bonds that control the frontier bands. The upper VB is predominately made up of the  $2p$  (O) states, but the states above  $0$  eV (localized states) are mostly of a nonbonding  $2p$  character from oxygen O1, the oxygen that loosens the connection with W2, as can be seen in Figure 1c. The consequence is a greater reduction of the gap energy to  $5.06$  eV due to the localized  $2p$  (O1) states.

Spectra a–c in Figure 6 illustrate the PL spectra recorded at room temperature for the BaWO<sub>4</sub> samples heat-treated at 500, 600, and 700 °C, respectively. They were excited by the  $488$  nm ( $\approx 2.54$  eV) line of an argon ion laser. The powders treated at



**Figure 5.** Calculated total and atom- and atomic orbital-projected densities of states (DOS) for the (a) BWO-c, (b) BWO-b, and (c) BWO-bw periodic models. The zero has been set to the Fermi energy calculated for the BWO-c model.

600 and 700 °C emit broad bands in the visible spectrum region, peaking in the green region. These broad bands are typical of a multiphonon process, that is, a system in which relaxation occurs by various paths, involving the participation of numerous states. The most intense PL emission is obtained for the structure that is neither highly disordered at short range (heat-treated at 500 °C) nor highly ordered (heat-treated at 700 °C), that is, for the sample treated at 600 °C.

The X-ray diffraction data and FT Raman and PL spectra show that the disorder at short range only of Ba in the crystalline BaWO<sub>4</sub> powder is a favorable and necessary condition for the most intense green PL emission in a scheelite lattice.

Table 2 presents the net charges of each molecular group of the three periodic models and their respective gap energies. The Ba<sub>2</sub>O<sub>6</sub> molecular group is formed by a barium atom (labeled Ba2 in Figure 1) and only six oxygen atoms due to the displacement of the Ba2 in the direction opposite to the oxygen atom labeled O2. The W<sub>2</sub>O<sub>3</sub> molecular group is formed by a tungsten atom labeled W2 and only three oxygens due the displacement of the W2 in the opposite direction to the oxygen labeled O1. The Ba<sub>1</sub>O<sub>8</sub>, Ba<sub>2</sub>O<sub>8</sub>, W<sub>1</sub>O<sub>4</sub>, and W<sub>2</sub>O<sub>4</sub> are regular molecular groups, as illustrated in Figure 1.

For the BWO-b model, the charge of the Ba<sub>2</sub>O<sub>6</sub> molecular group is positively increased by a local charge gain,  $\delta_b = +0.83 |e|$ ,

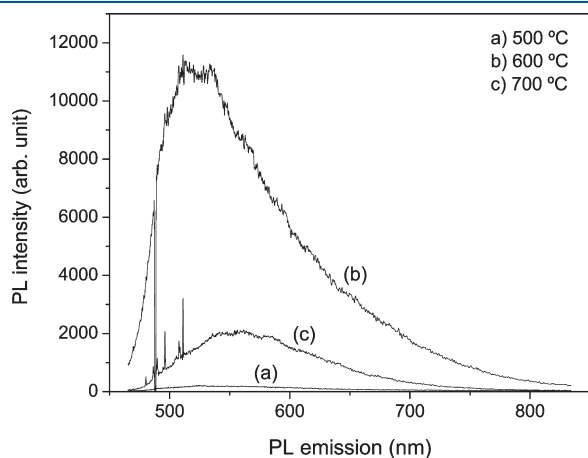


**Figure 6.** Photoluminescence spectra at room temperature of the BaWO<sub>4</sub> samples heat-treated at (a) 500, (b) 600, and (c) 700 °C.

and a large local electronic hole (trapped hole) is induced by the lost of connection with two oxygen anions, compensated by electron gains in the other molecular groups belonging to the unit cell.

For the BWO-bw model, the charge of the W<sub>2</sub>O<sub>3</sub> molecular group is positively increased by a local charge gain,  $\delta_{bw} = +0.24 |e|$ , and the W<sub>1</sub>O<sub>4</sub> group has a negative local charge gain,  $\delta_{bw} = -0.21 |e|$ . The charge in the Ba<sub>2</sub>O<sub>6</sub> molecular group is positively increased by a local charge gain,  $\delta_{bw} = +0.60 |e|$ . This charge gain of the Ba<sub>2</sub>O<sub>6</sub> molecular group is smaller than the charge gain of the Ba<sub>2</sub>O<sub>6</sub> group in the model BWO-b, because the displacement of W<sub>2</sub> tungsten induces a charge compensation. These results indicate that the trapped hole is larger in the case of one local deformation (BWO-b) than in the case of two local deformations (BWO-bw) in each unit cell due to the charge compensations by other adjacent molecular groups. This behavior indicates that the structures containing structural disorder at short range only of Ba have larger trapped holes and, consequently, are more favorable for intense PL emission, because bigger trapped holes are more favorable for attracting excited electrons to radiative recombinations when the lattice is submitted to photon excitation.

The structural transformations occur, by means of the polymeric precursor method, from disordered to ordered phases, starting from the early stage of the polyesterification of the citrate solution containing the tungsten and barium ions. The crystallization process occurs by heat treatment. The tungsten cation tends ideally to bond with four oxygen ions (WO<sub>4</sub>), and the barium cation tends ideally to bond with eight oxygen ions (BaO<sub>8</sub> pseudocubic configuration). The tungsten, which is more cationic, organizes sooner than the barium. In the structure just before the complete ordering at short range, there exist various coordination environments for the Ba, while the (WO<sub>4</sub>) tungsten molecular groups are already regular. The BaWO<sub>4</sub> structure annealed at 600 °C, the structure just before the complete ordering in which only the Ba are disordered at short range (see Figure 3, spectrum b), presented favorable conditions for the most intense PL emission (see Figure 6, spectrum b). When the high ordering is reached (sample treated at 700 °C), the WO<sub>4</sub> and BaO<sub>8</sub> molecular groups are highly regular (Figure 3, spectrum c) and the PL intensity considerably decreases (Figure 6, spectrum c), indicating that a complete order is not suitable to the most intense visible PL emission at room temperature in scheelite BaWO<sub>4</sub> crystals.

**Table 2.** Variation of Mulliken Charges for Each Molecular Group of the BWO Periodic Models and Their Respective Gap Energies

charge of the BWO-c molecular groups $ e $	charge of the BWO-b molecular groups $ e $	charge of the BWO-bw molecular groups $ e $
Ba <sub>1</sub> O <sub>8</sub> : -1.66	Ba <sub>1</sub> O <sub>8</sub> : -2.05	Ba <sub>1</sub> O <sub>8</sub> : -2.28
Ba <sub>2</sub> O <sub>8</sub> : -1.66	Ba <sub>2</sub> O <sub>6</sub> : -0.83	Ba <sub>2</sub> O <sub>6</sub> : -1.06
W <sub>1</sub> O <sub>4</sub> : 1.66	W <sub>1</sub> O <sub>4</sub> : 1.44	W <sub>1</sub> O <sub>4</sub> : 1.44
W <sub>2</sub> O <sub>4</sub> : 1.66	W <sub>2</sub> O <sub>4</sub> : 1.44	W <sub>2</sub> O <sub>3</sub> : 1.90
local charge gains $\delta_c$ of the BWO-c molecular groups $ e $	local charge gains $\delta_b$ of the BWO-b molecular groups $ e $	local charge gains $\delta_{bw}$ of the BWO-bw molecular groups $ e $
Ba <sub>1</sub> O <sub>8</sub> : 0.00	Ba <sub>1</sub> O <sub>8</sub> : -0.40	Ba <sub>1</sub> O <sub>8</sub> : -0.63
Ba <sub>2</sub> O <sub>8</sub> : 0.00	Ba <sub>2</sub> O <sub>6</sub> : +0.83	Ba <sub>2</sub> O <sub>6</sub> : +0.60
W <sub>1</sub> O <sub>4</sub> : 0.00	W <sub>1</sub> O <sub>4</sub> : -0.22	W <sub>1</sub> O <sub>4</sub> : -0.21
W <sub>2</sub> O <sub>4</sub> : 0.00	W <sub>2</sub> O <sub>4</sub> : -0.21	W <sub>2</sub> O <sub>3</sub> : +0.24
gap energy = 6.35 eV	gap energy = 6.29 eV	gap energy = 5.06 eV

The visible PL spectra show that the highly disordered and highly ordered structures at short range are not favorable to intense PL emission. It should be emphasized that the excitation energy used (2.54 eV, 488 nm) is smaller than that corresponding to the 420 nm ( $\approx 2.95$  eV) blue emission frequently attributed in the literature to the  $\text{WO}_4$  regular molecular group<sup>14,25,26,40,71</sup> and cannot be observed here for this reason.

The quantum-mechanical theory calculations and absorbance spectra analyses point out that the appearance of localized states in the band gap of  $\text{BaWO}_4$  structures and the increase of the structural disorder degree diminish the gap energy, as seen in Table 2 and Figure 4. The structural disorder can favor PL emission with excitation energy smaller than the crystalline gap energy. However, this sole effect alone is insufficient to enhance the intense visible PL at room temperature, as can be seen in the sample, which is more disordered at short range (treated at 500 °C), which does not present a PL intensity. The  $\text{BaWO}_4$  sample that presents the most intense PL emission (treated at 600 °C) has a higher experimental gap energy (4.1 eV) than the excitation energy used for collecting the PL spectra (2.54 eV, 488 nm). Such an observation confirms the fact pointed out by Montoncello et al.<sup>72</sup> that PL often highlights features that absorption measurements would rarely define, as the properties of the energy levels lying within the band gap of a material.

The charge gradient (polarization) and the presence of the localized states provide very good conditions for the trapping of electrons and holes, which can allow PL radiative recombination in the compounds containing simultaneous structural order and disorder. As explained by Blasse,<sup>13</sup> the PL arises from a radiative return to the ground state, a phenomenon that is enhanced by the presence of charge trapping at room temperature. Blasse indeed showed the PL behavior of perovskite-type oxides at low temperature (45 K), where less energy is lost for the vibration of the lattice so that the radiative recombination is encouraged. At room temperature, however, if no charge trapping promotes the radiative recombination, the energy is used for the lattice vibrations.

## CONCLUSIONS

The  $\text{BaWO}_4$  powders heat-treated at 500, 600, and 700 °C are already in the crystalline phase (structural order at long range), evidenced by means of XRD measurements.

Increasing structural ordering at short range of the  $\text{BaWO}_4$  powders by heat treatment from 500 to 700 °C was identified by means of FT Raman and absorbance spectra measurements.

FT Raman and PL emission spectra show that the highly crystalline  $\text{BaWO}_4$  powder presents a low PL emission intensity. The sample containing the highest structural disorder at short range presented a PL emission that was practically absent. The most intense and broad green PL emission was evidenced in the  $\text{BaWO}_4$  crystal containing short-range disorder only of Ba in the powder lattice.

The quantum-mechanical theory calculations evidenced that the  $\text{BaWO}_4$  crystal containing short-range disorder only of Ba presents large trapped electronic holes, indicating that this structure is more favorable for the PL emission, because larger trapped holes are more favorable for attracting excited electrons to radiative recombinations when the lattice is submitted to photon excitation.

The experimental and theoretical results show that the increase of green PL emission intensity is due to short-range structural disorder only of Ba in the crystalline  $\text{BaWO}_4$  lattice.

## ASSOCIATED CONTENT

**S Supporting Information.** Flow chart illustrating the procedure for the preparation of the  $\text{BaWO}_4$  solution and powder production. This material is available free of charge via the Internet at <http://pubs.acs.org>.

## AUTHOR INFORMATION

### Corresponding Author

\*E-mail: [marcos.anicete@hotmail.com](mailto:marcos.anicete@hotmail.com). Phone: +559132018235.

## ACKNOWLEDGMENT

The work was partially supported by the Brazilian agencies CNPq, CAPES, FAPESP, FAPESPA, PROPESP/UFPA, and FADESP.

## REFERENCES

- (1) Lee, A. J.; Pask, H. M.; Piper, J. A.; Zhang, H.; Wang, J. *Opt. Express* **2010**, *18*, 5984–5992.
- (2) Cerny, P.; Jelinkova, H.; Zverev, P. G.; Basiev, T. T. *Prog. Quantum Electron.* **2004**, *28*, 113–143.
- (3) Basiev, T. T.; Osiko, V. V.; Prokhorov, A. M.; Dianov, E. M. *Solid-State Mid-Infrared Laser Sources*; Topics in Applied Physics; 2003; Vol. 89, pp 351–396.
- (4) Zverev, P. G.; Basiev, T. T.; Sobol, A. A.; Skorniyakov, V. V.; Ivleva, L. I.; Polozkov, N. M.; Osiko, V. V. *Quantum Electron.* **2000**, *30*, 55–59.
- (5) Basiev, T. T.; Sobol, A. A.; Voronko, Y. K.; Zverev, P. G. *Opt. Mater.* **2000**, *15*, 205–216.
- (6) Basiev, T. T.; Sobol, A. A.; Zverev, P. G.; Osiko, V. V.; Powell, R. C. *Appl. Opt.* **1999**, *38*, 594–598.
- (7) Zverev, P. G.; Basiev, T. T.; Osiko, V. V.; Kulkov, A. M.; Voitsekhovskii, V. N.; Yakobson, V. E. *Opt. Mater.* **1999**, *11*, 315–334.
- (8) Basiev, T. T.; Sobol, A. A.; Zverev, P. G.; Ivleva, L. I.; Osiko, V. V.; Powell, R. C. *Opt. Mater.* **1999**, *11*, 307–314.
- (9) Du, S. F.; Shi, Y. X.; Zhang, D. X.; Li, Q. N.; Feng, B. H.; Zhang, J. Y.; Zang, J. C. *Opt. Commun.* **2009**, *282*, 2960–2963.
- (10) Cerny, P.; Zverev, P. G.; Jelinkova, H.; Basiev, T. T. *Opt. Commun.* **2000**, *177*, 397–404.
- (11) Kröger, F. A. *Some Aspects of the Luminescence of Solids*; Elsevier Publishing Company: Amsterdam, 1948.
- (12) Groeninck, J. A.; Blasse, G.; SOME, N. E. W. *J. Solid State Chem.* **1980**, *32*, 9–20.
- (13) Blasse, G.; Grabmaier, B. C. *Luminescent Materials*; Springer Verlag: Berlin, 1994.
- (14) Lecoq, P.; Dafinei, I.; Auffray, E.; Schneegans, M.; Korzhik, M. V.; Missevitch, O. V.; Pavlenko, V. B.; Fedorov, A. A.; Annenkov, A. N.; Kostylev, V. L.; Ligun, V. D. *Nucl. Instrum. Methods Phys. Res., Sect. A* **1995**, *365*, 291–298.
- (15) Belsky, A. N.; Mikhailin, V. V.; Vasilev, A. N.; Dafinei, I.; Lecoq, P.; Pedrini, C.; Chevallier, P.; Dhez, P.; Martin, P. *Chem. Phys. Lett.* **1995**, *243*, 552–558.
- (16) Nikl, M.; Nitsch, K.; Polak, K.; Mihokova, E.; Dafinei, I.; Auffray, E.; Lecoq, P.; Reiche, P.; Uecker, R.; Pazzi, G. P. *Phys. Status Solidi B* **1996**, *195*, 311–323.
- (17) Korzhik, M. V.; Pavlenko, V. B.; Timoschenko, T. N.; Katchanov, V. A.; Singovskii, A. V.; Annenkov, A. N.; Ligun, V. A.; Solskii, I. M.; Peigneux, J. P. *Phys. Status Solidi A* **1996**, *154*, 779–788.
- (18) Tamulaitis, G.; Buracas, S.; Martinov, V. P.; Ryzhikov, V. D.; Gutbrod, H. H.; Manko, V. I. *Phys. Status Solidi A* **1996**, *157*, 187–198.
- (19) Kobayashi, M.; Ishii, M.; Harada, K.; Usuki, Y.; Okuno, H.; Shimizu, H.; Yazawa, T. *Nucl. Instrum. Methods Phys. Res., Sect. A* **1996**, *373*, 333–346.

- (20) Zhu, R. Y.; Ma, D. A.; Newman, H. B.; Woody, C. L.; Kierstead, J. A.; Stoll, S. P.; Levy, P. W. *Nucl. Instrum. Methods Phys. Res., Sect. A* **1996**, *376*, 319–334.
- (21) Murk, V.; Nikl, M.; Mihokova, E.; Nitsch, K. J. *Phys.: Condens. Matter* **1997**, *9*, 249–256.
- (22) Millers, D.; Chernov, S.; Grigorjeva, L.; Pankratov, V. *Radiat. Meas.* **1998**, *29*, 263–266.
- (23) Nikl, M.; Strakova, P.; Nitsch, K.; Petricek, V.; Mucka, V.; Jarolimek, O.; Novak, J.; Fabeni, P. *Chem. Phys. Lett.* **1998**, *291*, 300–304.
- (24) Martini, M.; Meinardi, F.; Spinolo, G.; Vedda, A.; Nikl, M.; Usuki, Y. *Phys. Rev. B* **1999**, *60*, 4653–4658.
- (25) Shi, C. S.; Wei, Y. G.; Yang, X. Y.; Zhou, D. F.; Guo, C. X.; Liao, J. Y.; Tang, H. G. *Chem. Phys. Lett.* **2000**, *328*, 1–4.
- (26) Annenkov, A. A.; Korzhik, M. V.; Lecoq, P. *Nucl. Instrum. Methods Phys. Res., Sect. A* **2002**, *490*, 30–50.
- (27) Shang, H. M.; Wang, Y.; Bliss, M.; Cao, G. Z. *Appl. Phys. Lett.* **2005**, *87*, 051909.
- (28) Antonenko, O.; Chukova, O.; Hizhnyi, Y.; Nedilko, S.; Scherbatskiy, V. *Opt. Mater.* **2006**, *28*, 643–648.
- (29) Hernandez-Sanchez, B. A.; Boyle, T. J.; Pratt, H. D.; Rodriguez, M. A.; Brewer, L. N.; Dunphy, D. R. *Chem. Mater.* **2008**, *20*, 6643–6656.
- (30) Su, Y. G.; Li, L. P.; Li, G. S. *Chem. Mater.* **2008**, *20*, 6060–6067.
- (31) Zhang, F.; Sfeir, M. Y.; Misewich, J. A.; Wong, S. S. *Chem. Mater.* **2008**, *20*, 5500–5512.
- (32) Gu, J.; Zhu, Y.; Li, H.; Zhang, X.; Qian, Y. *J. Solid State Chem.* **2010**, *183*, 497–503.
- (33) Baryshevsky, V. G.; Korzhik, M. V.; Moroz, V. I.; Pavlenko, V. B.; Kobko, A. S.; Fyodorov, A. A.; Kachanov, V. A.; Solovjanov, V. L.; Zadneprovsky, B. I.; Nefyodov, V. A.; Nefyodov, P. V.; Dorogovin, B. A.; Nagornaja, L. L. *Nucl. Instrum. Methods Phys. Res., Sect. A* **1992**, *322*, 231–234.
- (34) Kobayashi, M.; Ishii, M.; Usuki, Y.; Yahagi, H. *Nucl. Instrum. Methods Phys. Res., Sect. A* **1993**, *333*, 429–433.
- (35) Blasse, G. *Chem. Mater.* **1994**, *6*, 1465–1475.
- (36) Lecoq, P. *Nucl. Instrum. Methods Phys. Res., Sect. A* **2005**, *537*, 15–21.
- (37) Zhang, Q. R.; Liu, T. Y.; Chen, J.; Feng, X. Q. *Phys. Rev. B* **2003**, *68*, 064101.
- (38) Anicete-Santos, M.; Orhan, E.; de Maurera, M. A. M. A.; Simoes, L. G. P.; Souza, A. G.; Pizani, P. S.; Leite, E. R.; Varela, J. A.; Andres, J.; Beltran, A.; Longo, E. *Phys. Rev. B* **2007**, *75*, 165105.
- (39) Guo, X.; Yang, J.; Deng, Y.; Wei, H.; Zhao, D. *Eur. J. Inorg. Chem.* **2010**, 1736–1742.
- (40) Qi, Z. M.; Shi, C. S.; Zhou, D. F.; Tang, H. G.; Liu, T.; Hu, T. D. *Physica B* **2001**, *307*, 45–50.
- (41) Baccaro, S.; Borgia, B.; Cecilia, A.; Dafinei, I.; Diemoz, M.; Fabeni, P.; Niki, M.; Martini, M.; Montecchi, M.; Pazzi, G.; Spinolo, G.; Vedda, A. *Nucl. Phys. B* **1998**, *61*, 66–70.
- (42) Sokolenko, E. V.; Zhukovskii, V. M.; Buyanova, E. S.; Krasnobaev, Y. A. *Inorg. Mater.* **1998**, *34*, 499–502.
- (43) Sinelnikov, B. M.; Sokolenko, E. V.; Zvekov, V. Y. *Inorg. Mater.* **1996**, *32*, 999–1001.
- (44) Chen, Y. H.; Shi, C. S.; Hu, G. Q. *J. Appl. Phys.* **2000**, *87*, 1503–1506.
- (45) Huang, Y. L.; Zhu, W. L.; Feng, X. Q. *J. Electron Spectrosc. Relat. Phenom.* **2003**, *133*, 39–45.
- (46) Ma, L.; Sun, Y.; Gao, P.; Yin, Y.; Qin, Z.; Zhou, B. *Mater. Lett.* **2010**, *64*, 1235–1237.
- (47) Cavalcante, L. S.; Sczancoski, J. C.; Lima, L. F.; Espinosa, J. W. M.; Pizani, P. S.; Varela, J. A.; Longo, E. *Cryst. Growth Des.* **2009**, *9*, 1002–1012.
- (48) Tyagi, M.; Sangeeta; Sabharwal, S. C. *J. Lumin.* **2008**, *128*, 1528–1532.
- (49) Chen, L.; Gao, Y.; Zhu, J. *Mater. Lett.* **2008**, *62*, 3434–3436.
- (50) Kakihana, M.; Okubo, T.; Arima, M.; Nakamura, Y.; Yashima, M.; Yoshimura, M. *J. Sol–Gel Sci. Technol.* **1998**, *12*, 95–109.
- (51) Kakihana, M.; Yoshimura, M. *Bull. Chem. Soc. Jpn.* **1999**, *72*, 1427–1443.
- (52) Lima, R. C.; Anicete-Santos, M.; Orhan, E.; Maurera, M. A. M. A.; Souza, A. G.; Pizani, P. S.; Leite, E. R.; Varela, J. A.; Longo, E. *J. Lumin.* **2007**, *126*, 741–746.
- (53) Saunders, V. R.; Dosevi, R.; Roetti, C.; Orlando, R.; Zicovich-Wilson, C. M.; Harrison, N. M.; Doll, K.; Civalieri, B.; Bush, I. J.; D’Arco, P.; Lluell, M. *Crystal03*; University of Torino: Torino, Italy, 2003.
- (54) Lee, C. T.; Yang, W. T.; Parr, R. G. *Phys. Rev. B* **1988**, *37*, 785–789.
- (55) Becke, A. D. *J. Chem. Phys.* **1993**, *98*, 5648–5652.
- (56) Hu, C. H.; Chong, D. P. *Encyclopedia of Computational Chemistry*; Wiley: Chichester, U.K., 1998.
- (57) <http://www.crystal.unito.it>.
- (58) Cabal, V. L. *OPTIM*; University of Oviedo: Oviedo, Spain, 1998.
- (59) Gurmen, E.; Daniels, E.; King, J. S. *J. Chem. Phys.* **1971**, *55*, 1093–1097.
- (60) Kokalj, A. *J. Mol. Graphics Modell.* **1999**, *17*, 176–179.
- (61) Anicete-Santos, M.; Picon, F. C.; Escote, M. T.; Leite, E. R.; Pizani, P. S.; Varela, J. A.; Longo, E. *Appl. Phys. Lett.* **2006**, *88*, 211913.
- (62) Orhan, E.; Anicete-Santos, M.; Maurera, M. A. M. A.; Pontes, F. M.; Paiva-Santos, C. O.; Souza, A. G.; Varela, J. A.; Pizani, P. S.; Longo, E. *Chem. Phys.* **2005**, *312*, 1–9.
- (63) de Figueiredo, A. T.; de Lazaro, S.; Longo, E.; Paris, E. C.; Varela, J. A.; Joya, M. R.; Pizani, P. S. *Chem. Mater.* **2006**, *18*, 2904–2911.
- (64) Orhan, E.; Varela, J. A.; Zenatti, A.; Gurgel, M. F. C.; Pontes, F. M.; Leite, E. R.; Longo, E.; Pizani, P. S.; Beltran, A.; Andres, J. *Phys. Rev. B* **2005**, *71*, 085113.
- (65) Longo, E.; Orhan, E.; Pontes, F. M.; Pinheiro, C. D.; Leite, E. R.; Varela, J.; Pizani, P.; Boschi, T.; Lanciotti, F.; Beltran, A.; Andres, J. *Phys. Rev. B* **2004**, *69*, 125115.
- (66) Orhan, E.; Pontes, F. M.; Leite, E. R.; Pizani, P. S.; Varela, J. A.; Longo, E. *ChemPhysChem* **2005**, *6*, 1530–1536.
- (67) Orhan, E.; Pontes, F. M.; Santos, M. A.; Leite, E. R.; Beltran, A.; Andres, J.; Boschi, T. M.; Pizani, P. S.; Varela, J. A.; Taft, C. A.; Longo, E. *J. Phys. Chem. B* **2004**, *108*, 9221–9227.
- (68) JCPDS, International Center for Diffraction Data, Card No. 8-4571400.
- (69) Wood, D. L.; Tauc, J. *Phys. Rev. B* **1972**, *5*, 3144–3151.
- (70) Porto, S. P. S.; Scott, J. F. *Phys. Rev.* **1967**, *157*, 716–719.
- (71) Vanloo, W. *Phys. Status Solidi A* **1975**, *27*, 565–574.
- (72) Montoncello, F.; Carotta, M. C.; Cavicchi, B.; Ferroni, M.; Giberti, A.; Guidi, V.; Malagu, C.; Martinelli, G.; Meinardi, F. *J. Appl. Phys.* **2003**, *94*, 1501–1505.